# Electromechanical Energy Conversion inside an Electromagnetic Vibratory Actuator: Modeling, Simulation, and Validation

**Uroš Lj. Ilić**
Research Assistant
University of Belgrade
Institute Mihajlo Pupin
Serbia

**Željko V. Despotović**
Principal Research Fellow
University of Belgrade
Institute Mihajlo Pupin
Serbia

**Mihailo P. Lazarević**
Full Professor
University of Belgrade
Faculty of Mechanical Engineering
Serbia

**Emil A. Veg**
Full Professor
University of Belgrade
Faculty of Mechanical Engineering
Serbia

*This paper covers the development and validation of a nonlinear mathematical model of an electromagnetic vibratory actuator used in vibratory conveyors. The motivation for this research stems from the need for a more detailed understanding of the electromechanical energy-conversion phenomena that occur during the operation of an electromagnetic vibratory actuator. Unlike previous mathematical models, which often use linear approximations or separately consider the mechanics and electrodynamics of the actuator, the proposed model integrates nonlinear electromagnetic effects with the dynamics of the electromagnet armature's relative motion, therefore establishing a dependence between the electrical quantities in the circuit and the dynamic characteristics of the moving element of the electromagnet. The newly developed mathematical model was simulated numerically, with the model parameters chosen based on a functional laboratory prototype. At the end, experimental validation is presented, demonstrating strong agreement with the simulation results.*

***Keywords:*** *Electromechanical energy conversion, Electromagnetic vibratory actuator, mathematical modelling.*

## 1. INTRODUCTION

The development of modern mechatronic systems requires a comprehensive approach that considers both mechanical and electromagnetic phenomena through several phases of system design [1,2]. A key element in the design of a machine is the development of its dynamic model, which enables engineers to evaluate the system's behavior using differential equations before physically integrating the machine. This early insight into potential system dynamics, energy flows, and performance limits—before building physical prototypes—reduces development time and minimizes production costs [3-7]. However, developing a highly accurate model of complex mechatronic systems presents a significant challenge. In addition to often complicated geometries and kinematic dependencies, the problem is further complicated by physical phenomena that cannot be described using linear equations. In such situations, numerical methods are often applied, including the finite element analysis (FEA), which provides a better insight into the potential dynamics of the system [8-11].

Electromagnetic actuators today represent key components of many mechatronic systems due to their ability to convert electrical energy into controlled mechanical motion [12,13]. A special group of these actuators is electromagnetic vibratory actuators (EVAs)that output controlled vibratory motion of the electromagnet armature [14-16]. In addition to the time-varying electromagnetic circuit, further nonlinearity is introduced by the spring's stiffness and damping, which return the working element to its initial position, hence providing oscillatory motion.

The efficiency of the electromechanical energy conversion process is influenced by both subsystems: the design of the electrical converter (i.e., the electromagnetic circuit equations) and the mechanical constraints of the moving components—stiffness, damping, and mass geometry [17,18]. Therefore, the development of an accurate mathematical model of EVA requires the consideration of coupled electromechanical phenomena, which include the behavior of the magnetic circuit, losses in the magnetic field, eddy currents, Joule losses, but also the armature's dynamics, spring stiffness and damping, various external dissipative effects, and workloads. Additionally, the development of a detailed actuator model, which includes the interaction between electrical and mechanical subsystems, would open up opportunities for the development of advanced automatic control algorithms, which aim to increase energy efficiency, i.e., by maintaining the vibratory regime in the areas of resonant frequencies, where the dissipative effects are the lowest.

Previous studies have examined various aspects of EVAs, but many of them simplify or decouple the interaction between the electrical and mechanical subsystems. For example, some mathematical models of EVAs, such as [17] assume constant inductance, while the author in [19] neglects coil resistance and treats the current as a controllablevariable. Other comprehensive mechanical models that include EVAs, although detailed in their mechanical formulation, omit electrical

Received: October 2025, Accepted: November 2025
Correspondence to: Uroš Ilić
University of Belgrade, Institute Mihajlo Pupin,
Volgina 15, 11060 Belgrade 35, Serbia
E-mail: uros.ilic@pupin.rs
**doi: 10.5937/fme2601023I**

current as a state variable or assume constant inductance [19,20]. However, despite the use of simplified and linearized mathematical models, several control algorithms have been developed, and the authors report that satisfactory performance was achieved [12,21]. In addition, there are purely theoretical conceptual studies that examine linear mechanical oscillators without any described practical implementation [22]. Overall, these studies typically address simplified oscillators with a single degree of freedom and do not consider the general case of motion, often neglecting gravity.

This paper describes the electromechanical energy conversion process in the EVA and presents a mathematical model formulation. Differential equations of relative motion of the armature are derived for the general case of vibratory motion. Numerical simulations were performed to provide insight into how the electrical quantities of the magnetic circuit change over time. Additionally, an experiment was conducted on a functional laboratory prototype of an electromagnetic vibrating conveyor. The measurement results are explained, and their correlation with numerical simulation results is described at the end of the paper.

## 2. ELECTROMECHANICAL ENERGY CONVERSION INSIDE THE EVA

The operation of the EVA can be understood through its coupled electrical and mechanical subsystems. The movable part of the mechanical subsystem comprises the movable armature, rigidly attached to the vibratory trough and supported by composite leaf springs (Fig. 1).The iron core with the corresponding coil of the EVA is rigidly connected to the massive base, which is separated from the ground with a set of rubber damping elements. The electromagnetic force generated by the EVA causes the vibratory trough to oscillate. In this way, electromagnetic energy is converted into mechanical energy, with most of it providing useful work, while the remainder is dissipated as losses.

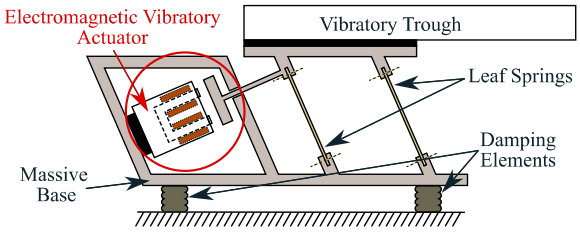


**Figure 1. The EVA positioning inside a vibratory conveyor**

The electrical subsystem includes the electromagnet and its control electronics, which generate a time-varying magnetic field in the coil. The interaction between the electrical and mechanical subsystems takes place through the air gap between the armature and the core: coil current variations produce pulses of electromagnetic excitation force, which provide mechanical movement, while the movement of the armature affects the change of the air gap, changing the magnetic field and the inductance of the EVA.

The magnetic field variation generates an electromagnetic force, acting on the movable armature and initiating motion in the mechanical system (Fig. 2). Its magnitude and temporal behavior depend on electrical excitation, core geometry, winding configuration, armature kinematics [20], and material properties of the armature and core as well [8,9].

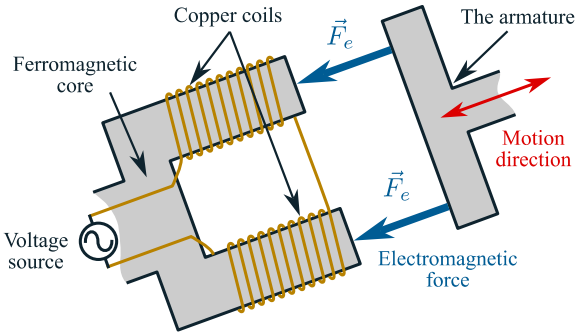


**Figure 2. The principle of operation of the EVA**

The conversion of electrical energy into mechanical energy within the EVA is rather a complex process and cannot be unambiguously formulated as a system of differential equations that directly relates one physical quantity to another [17,23]. In practice, various approximations of this process are frequently employed in the design of electrical machines [1,24]. Moreover, even in theoretical considerations, simplifications are often introduced, in order to obtain more practical analytical expressions [15,16].

The process of electromechanical energy conversion can be approximated by means of a block diagram, as illustrated in the Fig.3.

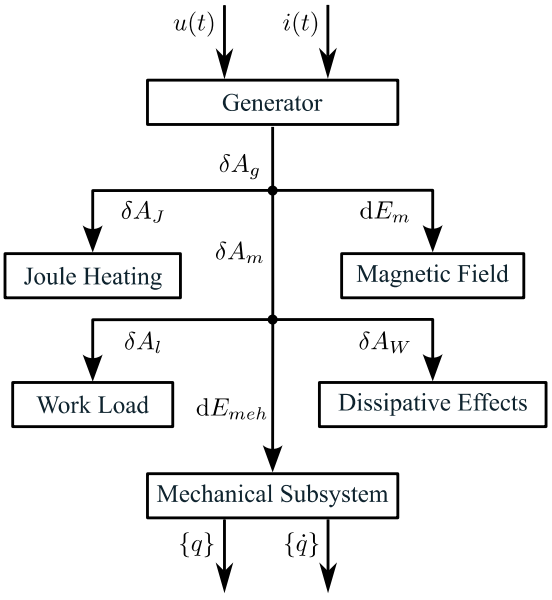


**Figure 3. The block diagram of the electromechanical energy conversion process that occurs inside the EVA**

With an electric current $i(t)$ and voltage $u(t)$, the voltage source, i.e., the electric generator, performs work $\delta A_g$. A portion of this work is dissipated as Joule losses, i.e., heat $(\delta A_J)$, while another portion contributes to the increase of magnetic energy $(\mathrm{d}E_m)$ and to the work done by magnetic forces $(\delta A_m)$ [15,16]. This process can also be mathematically formalized as follows:

$$\delta A_g = \delta A_J + \mathrm{d}E_m + \delta A_m \tag{1}$$

Energy is a state function, since it depends only on the initial and final state; thus, its change represents a total differential (denoted by the vertical letter 'd'). Work and heat, on the other hand, are process functions. They do not have a unique value between two states, since they depend on the process itself. Their changes are therefore not expressed as total differentials, and are denoted by the Greek letter δ. For additional explanation, the reader is guided to the relevant literature [25, 26].

In addition to Joule losses, other forms of energy dissipation occur within the electrical circuit, including magnetic core saturation, eddy currents, fringing effects, and magnetic flux leakage. These effects can be sufficiently mitigated by employing a magnetic material with a linear magnetization curve (to avoid saturation), by constructing the core from laminated sheets (to suppress eddy currents), by designing the core poles without sharp edges (to reduce fringing effects), and by ensuring that the air gap remains relatively small (to minimize flux leakage). Even when present, the significance of these losses is on the order of about 2% for specifictypical EVA configurations and can therefore be neglected [8,9].

In the context of dynamical modelling, these effects can be partially compensated by introducing a correction coefficient for the electromagnet's inductance [27]. While no general expression for this coefficient exists, an approximate value for a specific EVA design can be determined in other ways, for instance, by applying FEM-based computer-aided design tools (CAD) for electromagnetic field analysis. Still, numerical simulations offer a sufficiently accurate approximation of electromechanical energy conversion, with the added advantage of speed—taking only minutes compared to several hours for FEM analyses [28].

On the other hand, it is well known that the change in the mechanical energy of a system is equal to the work of the external forces acting upon it. In this case, the work $\delta A_m$ performed by the magnetic forces is primarily used to overcome the resistances encountered by the mechanical subsystem. These include various dissipative effects $(\delta A_W)$, such as dry and viscous friction, air resistance, and similar phenomena, as well as the external load work $(\delta A_l)$. Furthermore, a portion of the work of the magnetic forces contributes to the increase of the total energy of the mechanical subsystem $\mathrm{d}E_{mech}$, which may be expressed as:

$$\delta A_m = \delta A_W + \delta A_l + \mathrm{d}E_{meh} \tag{2}$$

The entire process of electromechanical energy conversion can be expressed in differential form by substituting (2)into(1). It follows that:

$$\delta A_g = \delta A_J + \mathrm{d}E_m + \delta A_W + \delta A_l + \mathrm{d}E_{meh} \tag{3}$$

One of the first steps in the mathematical modelling of a dynamical system is the identification of entities capable of storing energy [3-5]. During the considered process of electromechanical energy conversion, depicted in Fig. 3 and described by the energy balance equation given with(3), two such entities can be identified: the magnetic field and the mechanical subsystem. Once their states are known, the state of the electromechanical energy transducer, i.e., the EVA, is uniquely determined.

The magnetic field stores energy via the copper coil, while the mechanical subsystem stores energy as the kinetic energy of its moving parts and the potential energy of its spring-like elements. The research presented in this paper focuses on the electromechanical processes that occur in EVA during the general case of vibratory conveying.

## 3. DYNAMICAL MODEL OF THE ELECTRICAL SUBSYSTEM

The EVA, shown in Fig. 2 can be modeled as a magnetic circuit, that consists of a magnetic core and an armature, separated by two air gaps of equal length $l_z = D_0 + q$, where $D_0$ denotes the initial value of the air gap, and $q = q(t)$ represents the relative displacement of the actuator's armature [20]. Around the magnetic core, copper windings are wound to form a coil with a total of $N$ turns.

When an electric current $i = i(t)$ begins to flow through the copper windings, an electromagnetic field is generated in the vicinity of the coil. If the cross-sectional area of the core is equal to $A$, the total magnetic flux $\Phi_A$ through the cross-section of the core is equal to the product of the inductance $L$ of the electromagnet and the electric current $i(t)$ [15,16,20]. In this case, the inductance of the electromagnet that consists of two air gaps of equal lengths $l_z$ can be calculated as follows [17,20]:

$$L = L(q) = \frac{\mu_0 N^2 A}{2\left(D_0 + q(t)\right)} \tag{4}$$

where $\mu_0 = 4\pi \cdot 10^{-7}$ H/m . Furthermore, the change of inductance in time is equal to the first derivative of (4):

$$\frac{\mathrm{d}L(q)}{\mathrm{d}t} = -\frac{\mu_0 N^2 A}{2\left(D_0 + q(t)\right)^2}\dot{q}(t) \tag{5}$$

When the electric current flows through the copper windings, two electromagnetic phenomena occur—Joule losses and the induced electromotive force (EMF). Joule losses represent dissipative effects caused by the heating of the copper windings and are proportional to their resistance $R$, whereas the induced EMF is equal to the rate of change of magnetic flux through the considered cross-section of the magnetic circuit [15,16,20].

The EVA from Fig. 2 can also be represented as an R-L circuit. Hence, the voltage of the electrical generator, i.e., the source voltage $u_g = u_g(t)$ is equal to the sum of the voltage drop across the resistor and the induced EMF, namely [20]:

$$u_g = Ri + e_{ind} = Ri + \frac{\mathrm{d}\Phi_A}{\mathrm{d}t} = Ri + \frac{\mathrm{d}L}{\mathrm{d}t}i + L\frac{\mathrm{d}i}{\mathrm{d}t}, \tag{6}$$

which represents the final differential equation desc–ribing the change of electrical quantities in the elec–tromagnet shown in Fig. 2.

Various modeling approaches exist for electro–magnetic force, depending on system assumptions and complexity. A standard method assumes the force is proportional to the square of the current and inversely proportional to the square of the distance between moving parts [20,29]. Other models consider a linear combination of displacement, current, and their product to capture nonlinear electromechanical interactions [18, 30]. Numerical simulations and experiments confirm the nonlinear dependence, with force reduction roughly proportional to the square of the distance [6]. This re–search assumes that the magnitude of theforce generated due to the change in magnetic field energy can be calculated as follows [15,16,20]:

$$F_e = F_e(q,i) = \frac{\mu_0 N^2 A}{4\left(D_0 + q(t)\right)^2} i^2 \tag{7}$$

## 4. DYNAMICS OF THE MECHANCIAL SUBSYSTEM

The EVA is embedded within a mechanical system that, in general, is time-dependent in its motion. It would be unfounded to assume that the core of the electromagnet is stationary and to proceed by analyzing only the relative displacement between the armature and the ele–ctromagnetic core. By identifying the equation of general motion in an absolute coordinate system with the equation of relative motion in a non-inertial refe–rence frame, one would neglect inertial forces, which play a significant role in the armature's dynamics.

Furthermore, the armature of the electromagnet is not free to move in space (or plane), but rather cons–trained to a limited rectilinear trajectory of oscillatory character [31].

### 4.1 Analysisof the relative motion

Figure 4 depicts the EVA's armature in the form ofa free body diagram. The observed rigid body is located within the non-inertial coordinate system $B\xi\eta\zeta$, defined by the unit vectors $\vec{\lambda}$, $\vec{\mu}$, and $\vec{\nu}$. Its position relative to the absolute coordinate system $Oxyz$ is described by the position vector $\vec{r}_B$, the transmissive angular velocity $\vec{\omega}_p$, and the transmissiveangular acceleration $\vec{\varepsilon}_p$, which are indicated in green in Fig.4.

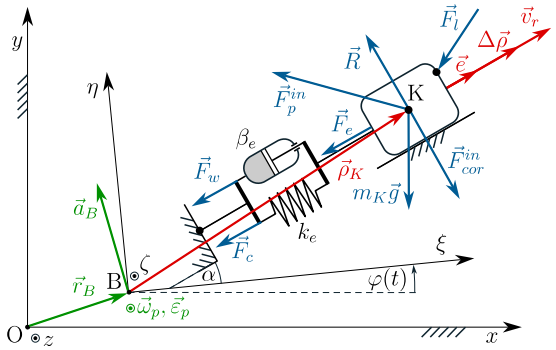


**Figure 4. The mechanics of the relative motion of the EVA's armature during the general case of vibratory transport**

For better comprehension of the origin and meaning of the vectors, the relevant vectors defining the kine–matics of the body within the non-inertial coordinate system—namely the corresponding displacements and velocities—are shown in red. Conversely, the vectors representing all forces acting on the body during its relative motion are depicted in blue.

Let the ferromagnetic core with copper windings be rigidly attached to the non-inertial coordinate system $B\xi\eta\zeta$. The working element of the electromagnet is the armature, whose mass, including all components rigidly connected to it, is denoted as $m_K$. The center of inertia of these components is located at point K. Suppose the armature of the considered electromagnet moves at an angle $\alpha$ with respect to the axis $B\xi$. In that case, the direction of relative motion can be represented by the local unit vector $\vec{e} = \cos\alpha \cdot \vec{\lambda} + \sin\alpha \cdot \vec{\mu}$ which can also be expressed as:

$$\vec{e} = \begin{pmatrix} \cos\alpha & \sin\alpha & 0 \end{pmatrix}^T \tag{8}$$

Since the armature undergoes rectilinear oscillatory motion, all points within its volume follow identical trajectories and are therefore subject to the same laws of relative motion dynamics as the material point $K$ [31]. The motion of the material point is considered within the non-inertial coordinate system $B\xi\eta\zeta$. Its motion with respect to the absolute coordinate system is defined by the position vector of its coordinate origin:

$$\vec{r}_B = \vec{r}_B(t) = x_B(t) \cdot \vec{i} + y_B(t) \cdot \vec{j} + z_B(t) \cdot \vec{k} \tag{9}$$

Since the motion is planar, for simplicity and wit–hout loss of generality, the analysis proceeds with $z_B = const = 0$. In this case, the translational velocity of the origin of the non-inertial coordinate system is gi–ven with $\vec{v}_B = (\dot{x}_B, \dot{y}_B, 0)^T$, while the translational acce–le–ration is $\vec{a}_B = (\ddot{x}_B, \ddot{y}_B, 0)^T$. Furthermore, because the motion is planar, the coordinate system $B\xi\eta\zeta$ posses–ses an angular velocity $\vec{\omega}_p = \dot{\varphi}\vec{k}$ and an angular acce–leration $\vec{\varepsilon}_p = \ddot{\varphi}\vec{k}$.

Hence, the position vector of the center of inertia of the movable part of the electromagnet in the absolute coordinate system is given with:

$$\vec{r}_K = \vec{r}_B + \vec{\rho}_K \tag{10}$$

where $\vec{r}_B$ is the position vector of point $B$ in the absolute coordinate system $Oxyz$, given with(9), and $\vec{\rho}_K$ is the position vector of point $K$ in the non-inertial coordinate system $B\xi\eta\zeta$. Since the given system performs an osci–llatory form of motion with a single degree of freedom, its motion can be represented by a single generalized coordinate $q(t)$. Accordingly, the change in the local position vector of any point on the body can be expressed as $\Delta\vec{\rho} = q(t)\vec{e}$, which, expressed in terms of its com–ponents in the local coordinate system, takes the form:

$$\{\Delta\vec{\rho}\} = q(t) \cdot \{\vec{e}\} = q(t) \begin{Bmatrix} \cos\alpha \\ \sin\alpha \\ 0 \end{Bmatrix} \tag{11}$$

thus, the relative position of point $K$ with respect to the origin of the local coordinate system can be expressed as:

$$\{\vec{\rho}_K\} = \{\vec{\rho}_{K,0}\} + \{\Delta\vec{\rho}\} = \begin{Bmatrix} \xi_{K,0} \\ \eta_{K,0} \\ 0 \end{Bmatrix} + q(t) \begin{Bmatrix} \cos\alpha \\ \sin\alpha \\ 0 \end{Bmatrix} = \begin{Bmatrix} \xi_{K,0} + q(t)\cos\alpha \\ \eta_{K,0} + q(t)\sin\alpha \\ 0 \end{Bmatrix} \quad (12)$$

where $\vec{\rho}_{K,0}$ denotes the position of point $K$ at the initial moment, i.e., when the electromagnet is at rest. In that case, the vectors of relative velocity and relative acceleration in the local coordinate system are given with

$$\{\vec{v}_r\} = \frac{\mathrm{d}}{\mathrm{d}t}\{\vec{\rho}_K\} = \dot{q}(t) \begin{Bmatrix} \cos\alpha \\ \sin\alpha \\ 0 \end{Bmatrix} \quad (13)$$

$$\{\vec{a}_r\} = \frac{\mathrm{d}^2}{\mathrm{d}t^2}\{\vec{\rho}_K\} = \ddot{q}(t) \begin{Bmatrix} \cos\alpha \\ \sin\alpha \\ 0 \end{Bmatrix} \quad (14)$$

where, for the sake of clarity, the subscript $K$ has been omitted in the notation for relative velocity and relative acceleration, since the motion is rectilinear and therefore all points on the armature possess identical velocities and accelerations.

Since the motion of the body in the relative coordinate system is of interest, it is necessary to express all vectors within the non-inertial coordinate system. The unit vectors of the absolute coordinate system, expressed in terms of the basis vectors of the moving coordinate system, are given as:

$$\begin{aligned} \vec{i} &= \cos\varphi\cdot\vec{\lambda} - \sin\varphi\cdot\vec{\mu} + 0\cdot\vec{\nu} \\ \vec{j} &= \sin\varphi\cdot\vec{\lambda} + \cos\varphi\cdot\vec{\mu} + 0\cdot\vec{\nu} \\ \vec{k} &= \quad 0\cdot\vec{\lambda} + \quad 0\cdot\vec{\mu} + 1\cdot\vec{\nu} \end{aligned} \quad (15)$$

which yields the coordinate transformation matrix from the absolute coordinate system $Oxyz$ to the relative coordinate system $B\xi\eta\zeta$ in the form:

$$[B] = \begin{bmatrix} \cos\varphi & \sin\varphi & 0 \\ -\sin\varphi & \cos\varphi & 0 \\ 0 & 0 & 1 \end{bmatrix} \quad (16)$$

The components of the translational acceleration vector $\vec{a}_B$, the angular velocity vector $\vec{\omega}_p$, and the angular acceleration vector $\vec{\varepsilon}_p$, which appear in the expressions for fictitious forces, are initially defined in the absolute coordinate system. They must be transformed into the non-inertial coordinate system $B\xi\eta\zeta$. Regarding the vector $\vec{a}_B$, its components in the relative coordinate system are given with:

$$\left\{\vec{a}_B^{(r)}\right\} = [B]\left\{\vec{a}_B^{(0)}\right\} = \begin{Bmatrix} \ddot{x}_B\cos\varphi + \ddot{y}_B\sin\varphi \\ -\ddot{x}_B\sin\varphi + \ddot{y}_B\cos\varphi \\ 0 \end{Bmatrix} \quad (17)$$

while the components of the vectors $\vec{\omega}_p$ and $\vec{\varepsilon}_p$ remain unchanged:

$$\left\{\vec{\omega}_p^{(r)}\right\} = [B]\left\{\vec{\omega}_p^{(0)}\right\} = \begin{Bmatrix} 0 \\ 0 \\ \dot{\varphi} \end{Bmatrix} \quad (18)$$

$$\left\{\vec{\varepsilon}_p^{(r)}\right\} = [B]\left\{\vec{\varepsilon}_p^{(0)}\right\} = \begin{Bmatrix} 0 \\ 0 \\ \ddot{\varphi} \end{Bmatrix} \quad (19)$$

which can be easily inferred by observing the arrangement of zero elements in the transformation matrix $[B]$ within (16). Since these operations involve vector cross products, it is more convenient to represent the vectors given with equalities (18) and (19) in form of their dual objects:

$$\left[\omega_p^d\right] = \begin{bmatrix} 0 & -\dot{\varphi} & 0 \\ \dot{\varphi} & 0 & 0 \\ 0 & 0 & 0 \end{bmatrix} \quad (20)$$

$$\left[\varepsilon_p^d\right] = \begin{bmatrix} 0 & -\ddot{\varphi} & 0 \\ \ddot{\varphi} & 0 & 0 \\ 0 & 0 & 0 \end{bmatrix} \quad (21)$$

### 4.2 Fundamental equation of the relative motion

The forces shown in the free-body diagram in Fig. 4 define the law of relative motion of the material point in the non-inertial coordinate system $B\xi\eta\zeta$. The funda–mental equation of dynamics for the relative motion of point $K$ in this case is given with:

$$m_K\vec{a}_r = \vec{R} + \vec{F}_e + \vec{F}_c + \vec{F}_w + \vec{F}_l + m_K\vec{g} + \vec{F}_p^{in} + \vec{F}_{cor}^{in} \quad (22)$$

Since the motion under consideration is rectilinear, the desired equation of motion can be obtained by projecting the aforementioned equation onto the direction of motion, which in this case is defined by the vector $\vec{e}$ that's defined with (8). Consequently, one can write:

$$\begin{aligned} m_K(\vec{a}_r)\cdot\{\vec{e}\} = &\left(\vec{R}\right)\cdot\{\vec{e}\} + \left(\vec{F}_e\right)\cdot\{\vec{e}\} + \left(\vec{F}_c\right)\cdot\{\vec{e}\} \\ &+ \left(\vec{F}_w\right)\cdot\{\vec{e}\} + \left(\vec{F}_l\right)\cdot\{\vec{e}\} + m_K(\vec{g})\cdot\{\vec{e}\} \\ &+ \left(\vec{F}_p^{in}\right)\cdot\{\vec{e}\} + \left(\vec{F}_{cor}^{in}\right)\cdot\{\vec{e}\} \end{aligned} \quad (23)$$

The left-hand side of equation (23) represents the acceleration of the armature in the non-inertial coordinate system, projected onto the direction of motion defined by the vector $\vec{e}$:

$$m_K(\vec{a}_r)\{\vec{e}\} = m_K\ddot{q}(t) \begin{Bmatrix} \cos\alpha \\ \sin\alpha \\ 0 \end{Bmatrix}^T \begin{Bmatrix} \cos\alpha \\ \sin\alpha \\ 0 \end{Bmatrix} = m_K\ddot{q}(t) \quad (24)$$

The right-hand side of (23)represents the total effect of the active and inertial forces acting on the armature. For subsequent analysis, the contribution of each force is determined individually, with each of them being multiplied scalarly by the vector $\vec{e}$.

### 4.3 Force analysis

During the motion of the body along the surface, the reaction force $\vec{R}$ can be decomposed into a normal

component, i.e., the surface reaction $\vec{N}$, and a horizontal component, i.e., the dry friction force $\vec{F}_\mu$.

During the deflection of the composite springs, the axial forces generated within the springs ensure the rectilinear motion [31]. Formally speaking, such a constraint can be classified as a restrictive, non-ideal, rheonomic (non-stationary), and non-holonomic (non-integrable) constraint [32].

Since viscous friction formally does not occur at the contact point between the armature and the constraint, the constraint can be represented as an ideal one, supplemented by an additional dissipative friction force, which is modelled separately in the form of a fictitious damping element with the damping coefficient $\beta_e$. Accordingly, the vector $\vec{R}$ is oriented perpendicularly to the direction of motion defined by the vector $\vec{e}$. Therefore, it follows that:

$$\left(\vec{R}\right)\{\vec{e}\} = 0, \tag{25}$$

which was to be expected, given the considerations above and the direction of the vector $\vec{R}$.

The electromagnetic force of the vibratory actuator $\vec{F}_e$ arises from changes in the energy within the magnetic field. It is collinear with the direction of the relative displacement of the armature, hence:

$$\left(\vec{F}_e\right)\{\vec{e}\} = -F_e(t)\begin{Bmatrix}\cos\alpha\\ \sin\alpha\\ 0\end{Bmatrix}^T\begin{Bmatrix}\cos\alpha\\ \sin\alpha\\ 0\end{Bmatrix} = -F_e(t) \tag{26}$$

The effect of the restitutive forces due to spring deformation is expressed through the vector $\vec{F}_c$. If the system contains a total of $l_c$ parallel springs with individual stiffness values $k_i$, the overall equivalent stiffness of the system will be $k_e = l_c \cdot k_c$. For the relative displacement of point $K$, defined by the vector $\Delta\vec{\rho}$ (given with (12)), its value is given as $\vec{F}_c = -k_e \cdot \Delta\vec{\rho}$ .By performing a scalar multiplication with the vector $\vec{e}$ (given with (8)), the total effect of the restitutive force due to the deformation of the composite springs is obtained:

$$\left(\vec{F}_c\right)\{\vec{e}\} = -k_e\left(\Delta\vec{\rho}\right)\{\vec{e}\} = -k_e q(t) \tag{27}$$

The vector $\vec{F}_w$ represents the main vector of the system's dissipative forces. Since the armature is surrounded by air, the only resistance to its motion comes from the aerodynamic drag force and the effect of viscous friction within the composite springs. Given that the velocities of the vibratory trough in steady-state vibratory regimes are not significant, the influence of aerodynamic drag during motion is neglected. On the other hand, the effects of viscous friction are more significant and are proportional to the relative velocity of the ends of the fictitious damper. In this case, that would be the relative velocity of point $K$. Therefore, the damping force of the system is expressed as $\vec{F}_w = -\beta_e \cdot \vec{v}_r$, where $\beta_e = l_c \cdot \beta_c$ represents the equivalent damping coefficient for $l_c$ parallel-arranged composite springs. Given that the relative velocity is always colinear with the unit vector $\vec{e}$ it follows that:

$$\left(\vec{F}_w\right)\{\vec{e}\} = -\beta_e\left(\vec{v}_r\right)\{\vec{e}\} = -\beta_e\dot{q}(t) \tag{28}$$

Following on, the effect of the external load is expressed through the vector $\vec{F}_l$, which acts on the electromagnetic armature during its relative motion. Its magnitude and direction are, in general, not deterministic quantities. Since its components in the non-inertial coordinate system are also time-dependent, i.e., $\vec{F}_l = \vec{F}_l(t) = F_{l,\xi}(t)\cdot\vec{\lambda} + F_{l,\eta}(t)\cdot\vec{\mu}$, its scalar product with the vector $\vec{e}$ is given with:

$$\begin{aligned}\left(\vec{F}_l\right)\{\vec{e}\} &= \begin{Bmatrix}F_{l,\xi}(t)\\ F_{l,\eta}(t)\\ 0\end{Bmatrix}^T\begin{Bmatrix}\cos\alpha\\ \sin\alpha\\ 0\end{Bmatrix}\\ &= F_{l,\xi}(t)\cos\alpha + F_{l,\eta}(t)\sin\alpha\end{aligned} \tag{29}$$

Additionally, since the armature has a significant mass, the effect of gravitational forces is represented by the vector $m_K\vec{g}$, where $\vec{g} = -g\cdot\vec{j}$. As $\vec{j}$ is the unit vector of the absolute coordinate system, the effect of gravitational forces needs to be converted to the relative coordinate system by multiplication with the transformation matrix [$B$] given with (16), and by multiplying scalarly with the vector $\vec{e}$, it follows:

$$m_K\left(\vec{g}^{(r)}\right)\{\vec{e}\} = m_K[B]\left(\vec{g}\right)\{\vec{e}\} = -m_K g\sin(\alpha+\varphi) \tag{30}$$

The effect of inertial forces acting on the body during its relative motion is expressed through the components of the transmissive inertial force $\vec{F}_p^{in}$ and the Coriolis force $\vec{F}_{cor}^{in}$.

The transmissive translational component of the inertial force is calculated using the formula $\vec{F}_{p,B}^{in} = -m\vec{a}_B$. By substituting the translational component of the transmissive acceleration given with (17), and multiplying scalarly with the vector $\vec{e}$, it follows:

$$\begin{aligned}\left(\vec{F}_{p,B}^{in}\right)\{\vec{e}\} &= -m_K\left(\vec{a}_B^{(r)}\right)\{\vec{e}\}\\ &= -m_K\left(\ddot{x}_B\cos(\alpha+\varphi) + \ddot{y}_B\sin(\alpha+\varphi)\right)\end{aligned} \tag{31}$$

Following on, the transmissive rotational component of the inertial force is calculated using the formula $\vec{F}_{p1}^{in} = -m_K(\vec{\varepsilon}_p \times \vec{\rho}_K)$, where the transmissive angular acceleration is expressed through its dual object from (21). By performing the vector cross product with the position vector of point $K$, given in (12), and perform scalar multiplication with the unit vector $\vec{e}$ it follows that:

$$\begin{aligned}\left(\vec{F}_{p1}^{in}\right)\{\vec{e}\} &= -m_K[\varepsilon_p^d]\left(\vec{\rho}_K\right)\{\vec{e}\}\\ &= -m_K\ddot{\varphi}(\xi_{K,0}\sin\alpha - \eta_{K,0}\cos\alpha).\end{aligned} \tag{32}$$

The centripetal component of the inertial force is given by $\vec{F}_{p2}^{in} = -m_K(\vec{\omega}_p \times (\vec{\omega}_p \times \vec{\rho}_K))$. If the transmis–

sive angular velocities are expressed using their dual objects given with (20) and relative position vector given with (12) and multiplied by the unit vector $\vec{e}$:

$$\left(\vec{F}_{p2}^{in}\right)\{\vec{e}\} = \left(-m_K[\omega_p^d]\times\left([\omega_p^d](\vec{\rho}_K)\right)\right)\{\vec{e}\} = m_K\left(\dot{\varphi}\right)^2(\xi_{K,0}\cos\alpha+\eta_{K,0}\sin\alpha+q) \quad (33)$$

The last component of the inertial force is the Co–riolis inertial force, which arises as a consequence of motion within a rotating coordinate system. It is cal–culated using the formula $\vec{F}_{cor}^{in} = -2m_K(\vec{\omega}_p\times\vec{v}_r)$. If the transmissive angular velocities are expressed using their dual objects given with (20), the expression of relative velocity (13) substituted and multiplied by a unit vector $\vec{e}$ the considered expression will evaluateto zero:

$$\left(\vec{F}_{cor}^{in}\right)\{\vec{e}\} = -2m_k[\omega_p^d](\vec{v}_r)\{\vec{e}\} = 0 \quad (34)$$

### 4.4 Differential equation of rectilinear motion of the EVA's armature

Differential equation of motion for the considered vibratory system can be obtained if expressions from previous subsections are substituted into (23). After rearrangement, the mentioned equation can be written down in the following form:

$$m_K\ddot{q}+\beta_e\dot{q}+k_eq = -F_e(t)+L_K(\varphi,t)+\Phi_K(\varphi,t), \quad (35)$$

where:

$$L_K(\varphi,t) = F_{l,\xi}(t)\cos\alpha+F_{l,\eta}(t)\sin\alpha - m_Kg\sin(\alpha+\varphi) \quad (36)$$

$$\Phi_K(\varphi,t) = -m_K\left(\ddot{x}_B\cos(\alpha+\varphi)+\ddot{y}_B\sin(\alpha+\varphi)\right) - m_K\ddot{\varphi}(\xi_{K,0}\sin\alpha-\eta_{K,0}\cos\alpha) + m_K\left(\dot{\varphi}\right)^2(\xi_{K,0}\cos\alpha+\eta_{K,0}\sin\alpha+q) \quad (37)$$

The right-hand side of the differential equation of motion for the single-degree-of-freedom oscillator, gi–ven with (35), represents the total excitation force acting on the oscillatory system. Here, the electromagnetic force of the vibratory actuator $F_e(t)$ is the only cont–rollable variable of the system. The remaining two terms on the right-hand side cannot be explicitly controlled during the operation of the vibratory actuator under standard operating conditions of the vibratory conveyor.

The term $L_K(\varphi,t)$ represents the influence of the electromagnetic actuator's working load. In addition to the working load, which is, in the general case, a non-deterministic quantity, the influence of gravitational forces is also included in the case where the actuator is not positioned horizontally ($\alpha \neq 0$). Even if it is positi–oned horizontally, the assumptions of rotation of the actuator in the vertical plane ($\varphi \neq 0$) brings gravitational acceleration into the effect.

The consequence of motion within a non-inertial coordinate system is captured by the scalar function $\Phi_K(\varphi,t)$. Put simply, when the vibratory actuator—i.e. the electromagnet—is embedded within a non-stationary mechanical assembly, additional (fictitious) forces arise that affect the actuator's dynamics. In other words, the governing law of the air gap variation is altered due to the presence of the electromagnetic force.

### 4.5 EVA as an exciting element inside the vibratory conveyor

The armature of the electromagnet is rigidly attached to the massive base of the vibratory conveyor. Theore–tically, point *B*, which represents the origin of the non-inertial coordinate system, can be placed anywhere in the absolute coordinate system *Oxyz*. Consequently, the relative position vector of point *K* inside the local coordinate system $B\xi\eta\zeta$ also changes, in accordance with (12). Therefore, let point *B* be located at the center of inertia of the massive base. Following the conc–lusions from [20,31,33] the physical interpretation of the symbolic quantities within (35) is as follows:

- The newly introduced generalized coordinate *q(t)*, which determines the relative displacement of the electromagnet armature, actually represents the fo–urth generalized coordinate of the considered sys–tem in [20,33], and its directly proportional to the size of the air gap inside the EVA.
- The variables $\ddot{x}_B$ and $\ddot{y}_B$ represent the orthogonal components of the transmissive acceleration of the center of inertia of the vibratory base. In this case, they are identical to the second time derivatives of the first two generalized coordinates from the afo–rementioned references.
- As a consequence of the coincidence of point *B* with the center of inertia of the massive base, the rotation angle $\varphi$ of the coordinate system $B\xi\eta\zeta$ represents the rotation angle of the massive base around its axis, i.e., the third generalized coordinate from the aforementioned references. Consequently, their derivatives are equivalent.
- The angle $\alpha$ defines the inclination of the elec–tromagnetic vibratory actuator relative to the hori–zontal plane. Since it is perpendicular to the leaf composite springs, it is also the angle formed by the springs with the vertical plane.
- The vector $\vec{\rho}_{K,0}$ defines the distance of point *K* from the center of inertia of the base at the initial moment. Its components $\xi_{K,0}$ and $\eta_{K,0}$ represent the horizontal and vertical distances, respectively. If the system is at rest at initial moment, absolute and relative coordinate systems' axes are parallel. Hence, for the sake of simplicity, and one can write $\xi_{K,0}\equiv\Delta_x$ and $\eta_{K,0}\equiv\Delta_y$.
- If the armature is connected to the electromagnet's core via a total of $l_c$ parallel composite springs, each with stiffness $k_c = 12\frac{EI}{L^3}$ [31] and damping coefficient $\beta_c$, the equivalent stiffness is $k_e = 12l_c\frac{EI}{L_c^3}$, and the equivalent damping coefficient is $\beta_e = l_c\beta_c$. In previous expression *E* represents

Young's modulus of elasticity of the leaf spring; $I$ isan axial moment of inertia around the bending axis and $L_c$ is the length of unclamped section of the spring.

Considering the cumulative effect of the inertial forces for the general case of relative motion of EVA, that's expressed with a scalar function given with (37), there are several ways to further simplify the differential equation of motion of the mechanical subsystem of the EVA, given with (35).

### 4.6 The assessment of the inertial force that acts on the EVA's armature

At the first glance, it is evident that the term $\ddot{x}_B \cos(\alpha+\varphi) + \ddot{y}_B \sin(\alpha+\varphi)$ originates from the translational acceleration of the center of inertia of the vibratory base, i.e., point *B*. The other two terms in (37) result from the rotation of the massive base around its axis. In addition to the angular velocity and angular acceleration, their magnitude is also influenced by the relative position of the centers of inertia of the massive base and the vibratory trough, as shown in Fig.5.

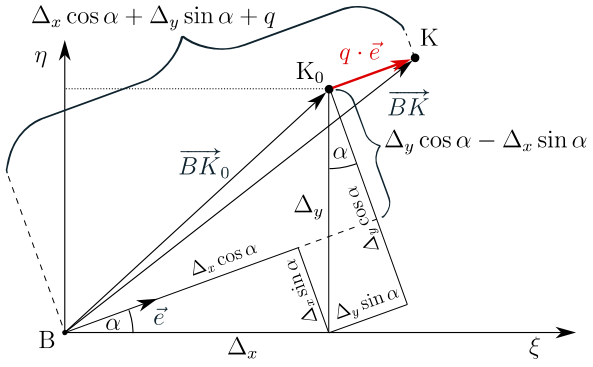


**Figure 5. Position of vibratory trough's center of inertia relative to base's center of inertia**

The transmissive centripetal component of the inertial force $(\vec{F}_{p1}^{in})$, in addition to the square of the angular velocity of the base, is largely defined by the term $(\Delta_x \cos\alpha + \Delta_y \sin\alpha + q)$, i.e., the distance between the centers of inertia of the trough and the base, projected onto the direction of motion. It is evident that, besides the relative displacement of point *K*, the centripetal component is also influenced by the position of the common center of inertia of all bodies rigidly attached to the armature, expressed by the aforementioned sum, which represents a constant value.

The transmissive component of inertial force ($\vec{F}_{p2}^{in}$) is mostly influenced by the angular acceleration of the vibratory base. It is multiplied by the length ($\Delta_x \sin\alpha - \Delta_y \cos\alpha$) which represents the distance between points *B* and *K*, perpendicular to the direction of displacement of the vibratory trough. From Fig. 5, it can be observed that this component is independent of the air gap's size and is determined solely by the geometry of the system. This transmissive component of the inertial force can be eliminated in two ways:

- If the base has no angular acceleration or it can be neglected, i.e. $\ddot{\varphi} \approx 0$, which further implies to $\varphi \approx 0$, since it is meaningless to speak of uniform rotational motion of a mechanical system such as a vibratory conveyor.
- If the vector $\overrightarrow{BK}$ coincides with the direction of motion of the electromagnet, defined by the unit vector $\vec{e}$. However, this problem should already be addressed during the mechanical design of the conveyor itself.

And finally, following previous consideration where angular velocity can be neglected ($\dot{\varphi} \approx 0$) the Coriolis force can be assumed zero, as well.

At the very least, by assuming that the electromagnet is placed on a stationary, horizontal, and flat surface $(\ddot{\varphi}, \dot{\varphi}, \varphi, \alpha = 0)$, eq. (35) reduces to:

$$m_K \ddot{q} + \beta_e \dot{q} + k_e q = -F_e(t) + F_{l,\xi}(t) - m_K \ddot{x}_B, \quad (38)$$

where the translational component of the transmissive inertial force remains, arising from the horizontal displacement of the ferromagnetic core of the electromagnet, i.e. $x_B = x_B(t)$. To properly account for this effect, one must either know the governing law of the core's displacement or introduce an additional differential equation, together with the mass of the electromagnet core. Such actuators are referred to as two-mass systems and are particularly suitable in applications where additional inertial forces are required, such as for mixing, shaking, or detaching material from the working element of a vibratory machine [18,29].

## 5. VALIDATION OF THE MATHEMATICAL MODEL

The differential equation describing the change of electrical quantities in the EVA, given with (6), together with the differential equation of the relative motion of the electromagnet armature, given with (35), provide the starting point for forming the mathematical model for the considered case of the EVA.

The process of electromechanical energy conversion can, to a certain extent, be modeled with satisfactory accuracy by introducing specific assumptions and approximations. For stable, low-intensity vibration regimes, where the damping elements are sufficiently stiff and the base mass is significantly larger than the mass of the vibrating structure, the displacements of the iron core are negligible compared to the displacements of the armature. Under these conditions, the core can be approximated as stationary, as done in [19,21].

On the other hand, modelling the influence of the transported material presents a significant challenge. In general, granular materials cannot be described by analytical expressions. Their behaviour must be modelled using methods based on statistical mechanics and material rheology [18], or by numerical and computational approaches [34,35]. For the purposes of validating the mathematical model of the EVA, the influence of the transported material will be neglected. However, in stable vibration regimes, this influence can be indirectly incorporated through a corrected damping coefficient, as shown in [19,21].

With respect to the aforementioned approximations and considerations (35) simplifies to the following form:

$$m_K\ddot{q} = -\beta_e\dot{q} + k_e q - F_e(t) - m_K g\sin\alpha \qquad (39)$$

In this situation, together with the electrical subsystem of the EVA, three fundamental forms of energy are distinguished, which define the state of the observed system:

- **Elastic potential energy**, which is being accumulated by the deformation of leaf springs. It's proportional to the armature's relative displacement from the initial position.
- **Kinetic energy** of the whole moving subsystem; considering the approximations above, it can be calculated using the relative velocity of the armature, considering that the overall mass of this subsystem is equal to $m_k$.
- **Magnetic energy**, that's being predominantly accumulated inside the air gap. It's mostly effected by the intensity of the electric current that flows through coils.

### 5.1 Mathematical model for the considered EVA

For a successful formulation of the mathematical model, it is necessary that the proposed system possesses as many state variables as there are entities capable of storing energy [17,36]. Considering that the observed electromechanical system contains three elements capable of storing energy, it is necessary to define three state variables, that will describe the system's state at each moment:

1. Relative displacement: $x_1(t) = q(t)$;
2. Relative velocity of the armature: $x_2(t) = v_r(t)$
3. Electrical current in the coil: $x_3(t) = i(t)$;

which require definition of three separate state equations. Given that $v_r(t) = \dot{q}(t)$, the first state equation can be formulated as follows:

$$\frac{\mathrm{d}x_1}{\mathrm{d}t} = x_2(t) \qquad (40)$$

Following on, the second state equation can be obtained if the expression for electromagnetic force from (7)is substituted into (39)and state variables are replaced:

$$\frac{\mathrm{d}x_2}{\mathrm{d}t} = -\frac{\beta_e}{m_K}x_2 - \frac{k_e}{m_K}x_1 - \frac{\mu_0 N^2 A}{4(D_0 + x_1)^2}x_3^2 - m_K g\sin\alpha \qquad (41)$$

Final, third equation ought to define dynamics of the electrical current that runs through the copper coils of the EVA, hence forming the electromagnetic field around it. For this purpose, eq. (6) can be rearranged as follows:

$$\frac{\mathrm{d}i}{\mathrm{d}t} = L^{-1}\left[u_g(t) - i\left(R + \frac{dL}{dt}\right)\right], \qquad (42)$$

which, after the substitutions for inductance and its first derivative with their expressions from (4) and (5), and swapping for aforementioned state variables, evaluates to:

$$\frac{\mathrm{d}x_3}{\mathrm{d}t} = \frac{D_0 + x_1}{\mu_0 N^2 A}\left[x_3\left(\frac{\mu_0 N^2 A}{(D_0 + x_1)^2}x_2 - R\right) + u_g(t)\right] \qquad (43)$$

Furthermore, if the state vector and its first derivative are introduced as:

$$X = \begin{pmatrix} x_1 & x_2 & x_3 \end{pmatrix}^T; \quad \dot{X} = \begin{pmatrix} \frac{\mathrm{d}x_1}{\mathrm{d}t} & \frac{\mathrm{d}x_2}{\mathrm{d}t} & \frac{\mathrm{d}x_3}{\mathrm{d}t} \end{pmatrix}^T, \qquad (44)$$

the system of differential equation given with (40), (41) and (43) can be also written in a compact form, which is more suitable for computer, i.e. numeric computations:

$$\dot{X} = A(X) + B(X)\cdot U(t), \qquad (45)$$

where:

$$A(X) = \begin{Bmatrix} x_2 \\ -\frac{\beta_e}{m}x_2 - \frac{k_e}{m}x_1 - \frac{\mu_0 N^2 A}{4(D_0 + x_1)^2}x_3^2 - m_k g\sin\alpha \\ \frac{D_0 + x_1}{\mu_0 N^2 A}x_3\left(\frac{\mu_0 N^2 A}{(D_0 + x_1)^2}x_2 - R\right) \end{Bmatrix} \qquad (46)$$

and

$$B(X) = \frac{D_0 + x_1}{\mu_0 N^2 A}; \quad U(t) = \begin{Bmatrix} 0 \\ 0 \\ u_g(t) \end{Bmatrix} \qquad (47)$$

### 5.2 Description of the laboratory setup and definition of model parameters

The proposed mathematical model of the electromagnetic vibration actuator was validated on a functional prototype of a vibratory conveyor realized in the Mechatronics laboratory of the Institute Mihajlo Pupin. The prototype has a total mass of the vibrating trough of $m_K$ = 0.83kg, while the initial air gap is $D_0$ = 4.7 mm. The vibrating base is rigidly fixed to a massive iron ballast, minimizing its displacements and allowing it to be considered stationary during the operation of the EVA, as shown in Fig. 6.

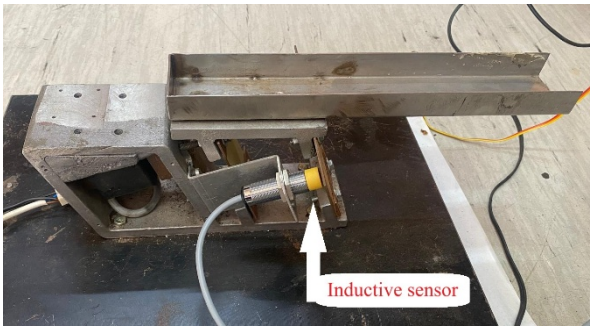


**Figure 6. The laboratory prototype of the considered vibratory conveyor with an inductive sensor attached**

The relative displacements of the vibrating trough were measured using an inductive sensor *Ni10-18-LiU-H1141* manufactured by *Turck*. The placement of this sensor is also shown in the Fig. 6. This sensor provides

a linear output voltage in the range of 0.05–10V corresponding to relative displacements from 0.5–4mm More precisely, within the linear measurement range, a unit change in voltage corresponds to an exact relative displacement of 0.352mm.

To determine the dynamic characteristics of the vibrating conveyor, an experimental study was con–ducted involving pulse mechanical excitation of the system. In this case, a short mechanical impulse was introduced to the system in the direction of the relative displacement of the armature of the electromagnetic vibrating actuator, which induced a response in the form of free damped oscillations. The response was measured using the aforementioned inductive sensor, and the analog signal was recorded with a high-resolution digital oscilloscope (Fig. 7).

A Fast Fourier Transform (FFT) was applied to the measurement data to examine the frequency com–ponents of the free damped oscillations of the vibratory trough. The resulting natural frequency of the observed system equals to $f_n$ = 55Hz which will be used as the excitation frequency for both the numerical simulations and the following laboratory tests.

Following on, the damping ratio of damped vib–rations can be calculated using the logarithmic decre–ment. Despite the fluctuations that occur as an effect of AC/DC conversion of the input signal, the average damping ratio was calculated to be $\zeta_e \approx 0.028$. This estimation can be considered as valid given that typical viscous damping ratios for composite leaf springs take value from 1% to 5% [37], [38].

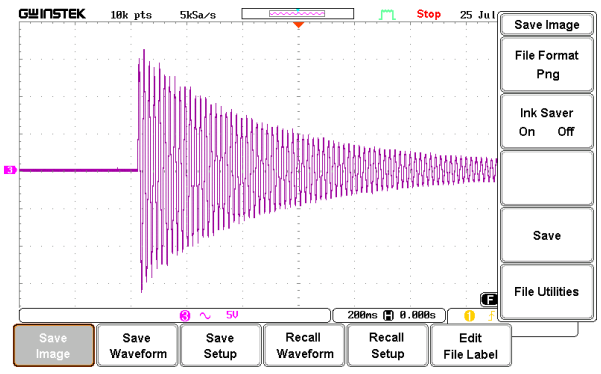


**Figure 7. System's response after a mechanical impulse alongside the relative displacement of the EVA**

For the oscillating mass of $m_K$ = 0.83kg and linear frequency of $f_n$ = 55Hz, i.e. angular frequency $\omega_n = 2\pi f_n$ = 345.6 rad/s, the equivalent stiffness and damping of the system equates to:

$$k_e = \omega_n^2 \cdot m_K = 99134.67\text{N/m} \approx 99135\text{N/m} \quad (48)$$

$$\beta_e = 2\zeta_e\sqrt{k_e m_K} = 15.91\text{N/(m/s)} \quad (49)$$

The schematic of power converter circuit supplying the EVA coils is depicted in Fig.8. Measurements taken at the EVA's terminals showed the electromagnet's resistance and inductance to be $R$ = 96Ω and $L_0$ = 1.56H, respectively, where the index *0* indicates that the measurements were taken at initial moment. While the coil's number of turns $N$ and the effective cross-sectional area of the air gap $S$ could not be directly measured, their combined effect was inferred from their combined influence, as follows:

$$AN^2 = \frac{2D_0L_0}{\mu_0} = \frac{2\cdot 4.7\text{mm}\cdot 1.56\text{H}}{4\pi\cdot 10^{-7}\,\text{H/m}} = 11669.24\text{m}^2 \quad (50)$$

A constant supply voltage of $V_g$ = 300V is applied. The control unit includes two switches, *S1* and *S2*, which are driven by a pulse width modulation signal (PWM). When both switches are closed, current intensity rises through the coils due to the applied positive voltage. After opening the switches, the magnetic energy stored in the EVA coils is returned through the freewheeling diodes *D1* and *D2* in the power source $V_g$.

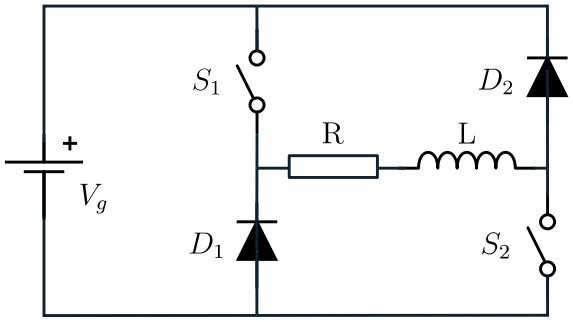


**Figure 8. The schematic of power converter circuit for supplying the EVA**

The voltage applied to the EVA can be modelled as follows [19]:

$$u_g(t) = \begin{cases} V_g, & u_D = 1 \\ -V_g, & (u_D = 0) \wedge (i(t) > 0) \\ 0, & \text{otherwise} \end{cases} \quad (51)$$

where $V_g$ denotes the voltage source, and $u_D$ is the output of the PWM control function with frequency $f_n$ and an adjustable preset duty cycle $\delta$, which determines the width of the applied voltage pulse.

For enhanced clarity parameters that constitute the mathematical model of EVA given with (45) are given in Table 1.

**Table 1. Parameter values used for numerical simulation**

| Parameter name | Value |
|---|---|
| Oscillating mass $m_k$ | 0.83kg |
| Equivalent damping coefficient $\beta_e$ | 15.91N(m/s) |
| Equivalent stiffness $k_e$ | 99135N/m |
| Number of turns × cross section $N^2A$ | 11669.24m$^2$ |
| Initial length of the air gap $D_0$ | 4.7mm |
| Resistance of the copper coil $R$ | 96Ω |
| Initial inductance of the copper coil $L_0$ | 1.56H |
| Supply voltage $V_g$ | 300V |
| Duty cycle $\delta$ | 10% |
| Driving frequency $f_n$ | 55Hz |

Following on, the initial state of the system needs to be defined as well. Due to the weight of the vibratory trough and all components rigidly attached to it, the value of the air gap at the initial moment is reduced by:

$$q_0 = -\frac{m_K g \sin\alpha}{k_e} = -3,385 \cdot 10^{-5}\,\text{m}, \qquad (52)$$

and given the fact that the armature starts from the state of rest and that the initial electrical current is equal to zero, the state vector at the initial moment takes following value:

$$X_0 = \begin{pmatrix} -3.385 \cdot 10^{-5} & 0 & 0 \end{pmatrix}^T \qquad (53)$$

Both the numerical simulation and laboratory experiment will be performed with lesser excitation magnitudes, i.e. the vibrations will be near the system's equilibrium point. Although inductance varies drastically with slight displacements, leaf springs' stiffness can be assumed constant for relatively small bending. For larger bending angles, stiffness becomes nonlinear and the trough deviates from a rectangular path, i.e., its motion can't be considered as rectilinear anymore [31].

Furthermore, given that the vibratory trough moves rectilinearly, the inductive sensor measures the distance to a surface that remains parallel to its tip, yielding valid measurements.

## 6. NUMERICAL SIMULATION RESULTS

Figure 9 shows one impulse of the electrical current. It depicts the dependence between electrical values in the circuit from Fig. 8. Upon application of voltage to the vibratory actuator terminals (R-L circuit), $e_{ind}$ abruptly rises to 300V then gradually decreases as the electrical current increases, reaching 269.25V, which corresponds precisely to the difference between the source voltage and the Joule losses given by $R \cdot i$ at that instant.

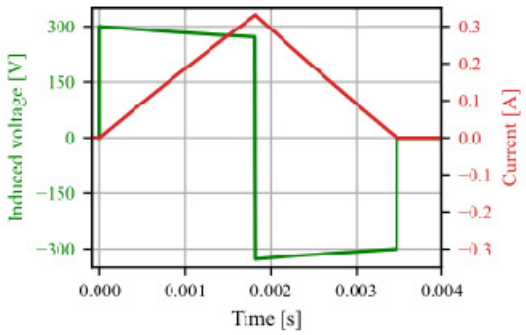


**Figure 9. Changes in electrical current and induced voltage during one period of the resonant vibratory regime**

After control signal opens the switches, the current starts decreasing, and the value of the induced voltage drops instantaneously to -330.3V , then gradually rises until the electrical current drops to zero. After this moment, there is no electrical current in the copper coil, hence the induced voltage drops to zero. One period lasts for exactly 36.36ms. After multiple consecutive impulses, the armature starts the desired vibratory motion. Figure 10 illustrates the process of reaching a steady-state vibratory regime under excitation by an impulse-shaped resonant frequency. The blue curve represents the relative displacements of the EVA's armature $q(t)$, while the red curve corresponds to the sequence of current pulses.

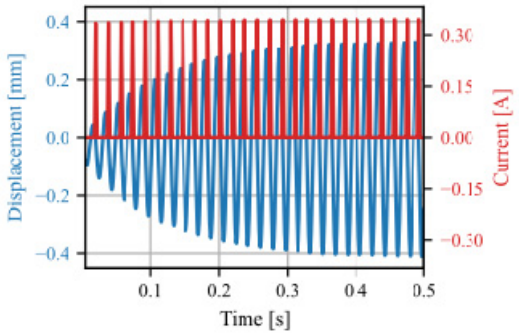


**Figure 10. The gradual rise of vibration amplitudes during the initial phase of the resonant vibratory regime**

During the initial phase, the vibration amplitudes gradually increase because the energy input exceeds the energy lost due to dissipative effects (viscous friction and Joule heating). Since viscous damping is proportional to the armature velocity, energy dissipation grows as the velocity amplitude rises. Eventually, the system reaches a stable vibratory regime in which excitation and dissipation are balanced, and the oscillations stabilize. For a given vibratory regime, the oscillations stabilize at peak-to-peak values of 0.74mm.

The presented graph illustrates the essence of a resonant vibratory regime - the system receives exactly the amount of energy required to compensate for dissipative losses. In this regime, current pulses occur as the armature passes through the equilibrium position during the return stroke. This phenomenon is even more clearly observed in Fig. 11, where several oscillation periods are magnified. In addition to current and displacement, the translational velocity of the armature, $\dot{q}(t)$, is shown in orange. It can be observed that the electrical current peaks exactly when the translational velocity of the armature attains its maximum amplitude - occurring exactly at the moment the armature passes through the equilibrium position.

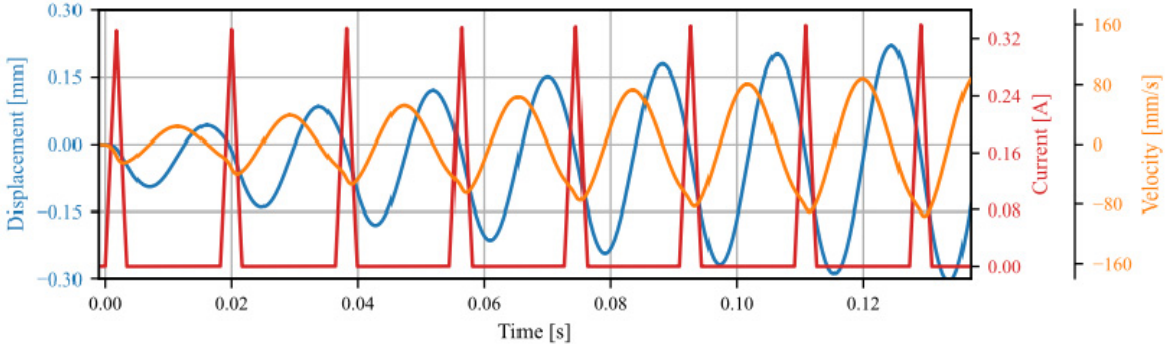


**Figure 11. Displacement, velocity and electrical current during the transient phase of resonant vibratory regime**

For better comprehension of the electromagnetic processes that occur inside the EVA, Fig. 12illustrates the change of all significant electromagnetic quantities during the observed resonant vibratory regime. The simulated source voltage is shown in navy blue; it should be noted that the actual source voltage does not have negative halves, and the function $u_g$ represents solely the result of the piecewise function given with (51). At the moment when $u_g$ changes sign, the current (red) reaches a maximum value of 0.33A . The trian–gular current pulse corresponds to the triangular pulse of the magnetic flux $\Phi_A$ , depicted in light blue, reaching a maximum of 0.515T. As mentioned before, the first derivative of the magnetic flux represents the induced voltage at the electromagnet terminals $e_{ind}$, which shown in green.

The remaining three terms that constitute the induced EMF expression — the electromagnet induc–tance, its first derivative, and the time derivative of the current — are shown in olive green, purple, and pink, respectively. It can be observed that the variation of the inductance follows a sinusoidal pattern, inversely proportional to the sinusoid of the armature relative displacement. In other words, when the armature is closest to the core, the inductance reaches its maximum, as expected from(4). Moreover, the first derivative of the inductance, according to(5), partially resembles the shape of the armature relative velocity. Deviations from the ideal sinusoidal shape are noticeable at the moments of the current pulse, identical to those observed in the relative velocity graph in Fig. 10.

## 7. EXPERIMENTAL VALIDATION

The validity of the proposed mathematical model was tested using the previously described laboratory prototype. The pulse frequency was set to $f_n$ = 55Hz with a duty cycle of $\delta$ = 10%. A screenshot from the oscilloscope showing the vibratory regime, with a horizontal time scale of 5ms per division, i.e. 5ms/div. The displacement signal from the inductive sensor is presented in Fig. 13. In addition to the displacement signal, the oscilloscope also monitored the electrical current and voltage across the electromagnet.

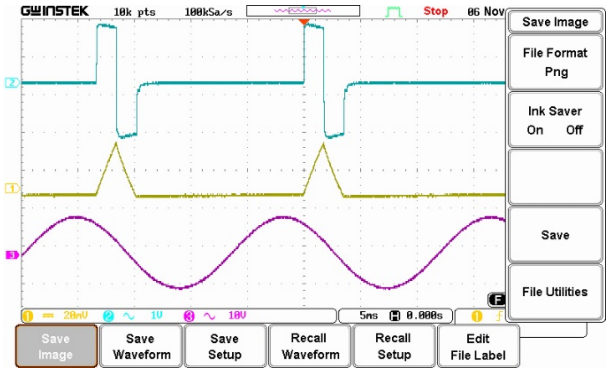


**Figure 13. Current (yellow), voltage (blue) and the displace–ment (purple) during the experimental resonant regime of the vibratory conveyor**

The probe that measured the electrical current has a transfer characteristic of 0.1A/10mV and was monitored on channel CH1 with a vertical scale of 20mV/div. In this configuration, the height of one division of the current signal corresponds to 0.2A. The voltage probe, on the other hand, has a 200:1 attenuation ratio. Since the voltage was recorded on channel CH2 with a vertical scale of 1V/div one oscilloscope division corresponds to 200V of the measured signal.

The voltage signal from the inductive displacement sensor was amplified, giving a scale of 10V/div. Considering the sensor's transfer ratio, this amounts to a total sensor division of 0.352mm/div. The zero point in Fig. 13 is set to clearly indicate the time intervals bet–ween two switch closures, corresponding to consecutive voltage jumps from 0 to 300V, which span slightly over 3.6 divisions, corresponding to 18.182 ms.

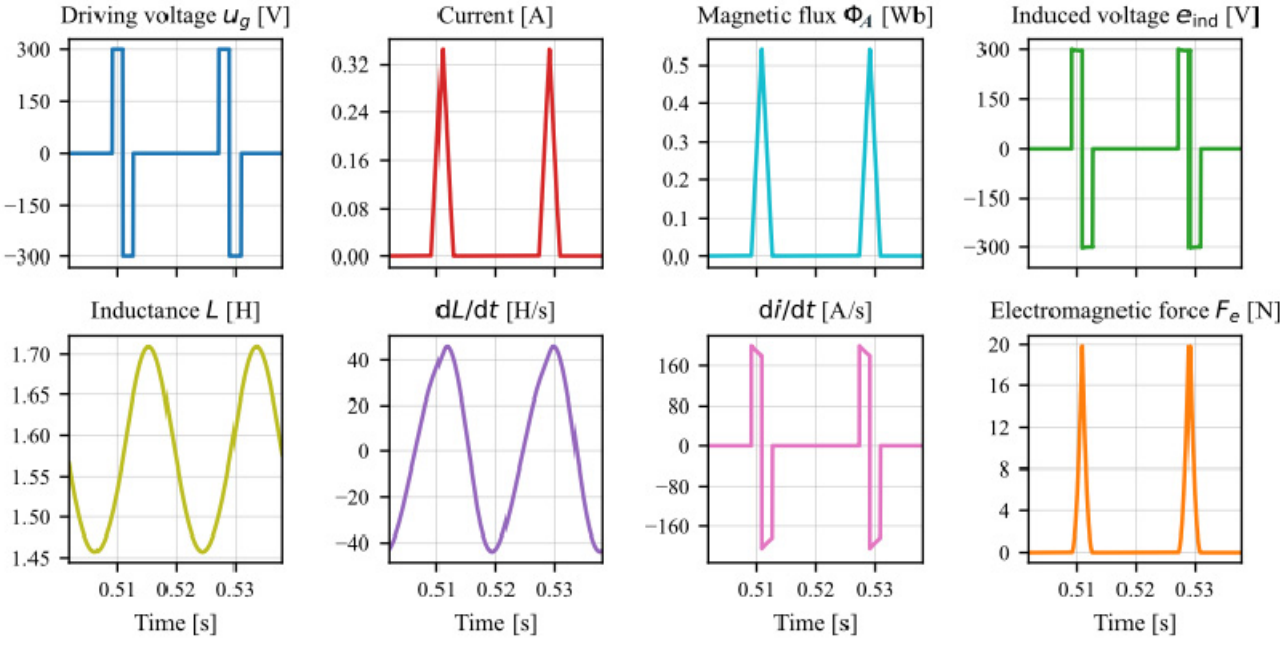


**Figure 12. Changes in significant electromagnetic quantities during the operation of the EVA**

For better clarity, Fig. 14 shows an enlarged view of one oscillation period with a time scale of 2ms/div where the peak of the electrical current pulse coincides with the moment the armature passes through its equi–librium position during the return stroke of the vibratory trough. In the observed resonant regime shown in Fig. 14, the displacement signal oscillates over approxi–mately 1.9 divisions, which correspondsto a working stroke of 0.669mm and oscillation amplitudes of approx. 0.345mm.

After the switching circuit closes, the voltage signal rises for about 1.5div, which corresponds to 300V. At this moment, the current also begins to increase with a slightly exponential characteristic. As the current rises, the voltage across the electromagnet decreases, consis–tent with the expected Joule losses in the circuit. Alt–hough the sampling rate during oscilloscope digitization is not particularly high, it can be observed that the voltage drops by approximately. 0.1div, i.e. roughly 20V. After 1.8ms , the switches open again, causing the voltage to abruptly fall by exactly -600V , i.e.three vertical divisions.Within this oscillation regime, the triangular current pulse peaks at exactly 1.5 div, corresponding to approximately 0.3A.

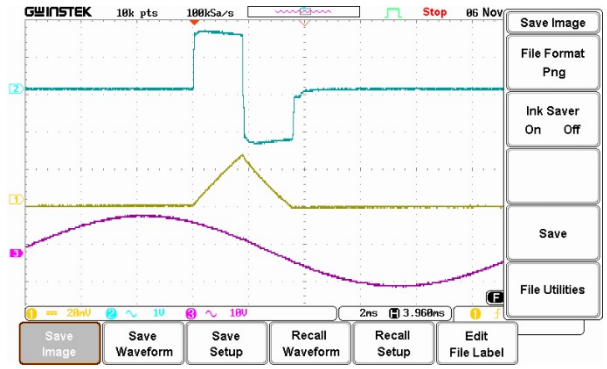


**Figure 14. The coincidence of current's peak values (yel–low) and voltage (blue) switching moment with an equilib–rium point of the vibratory trough (purple) during the reso–nant vibratory regime**

### 7.1 Comparison between experimental and simulation results

This subsection presents a brief discussion of the cor–relation between simulated results and experimental values. The oscilloscope readings that were shown in Fig. 13 were exported in .csv format and post-proces–sed. Given that Fig. 13 depicts a stable vibratory regime, the simulation results were taken after the transient period of 0.5s (as shown in Fig. 10). The corresponding curves were manually aligned; hence, there is no temporal axis enumeration in the following figures.

Figure 15 depicts the comparison between actual (measured) and simulated displacement of the vibratory trough. Measured displacement values oscillate between -0.36mm and 0.31mm, while simulated values oscillate in the range between -0.41mm and 0.33mm. This equates to a working stroke of 0.67mm and an estimated one of 0.74mm.

Following this, the resemblance between the simu–lated and actual induced voltages on the electromagnet is shown in Fig. 16. Simulated impulses match the shape and width of the actual ones. The voltage drop due to Joule heating is somewhat similar, even though the actual voltage drop is lower when the polarity reverses, i.e., when the switches return to the open position.

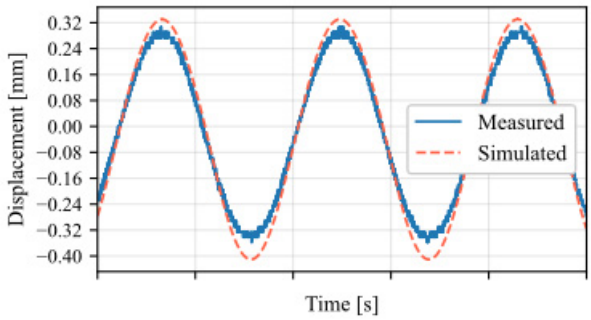


**Figure 15. Comparison between measured (blue) and simulated (dashed red) values of the trough's displacement**

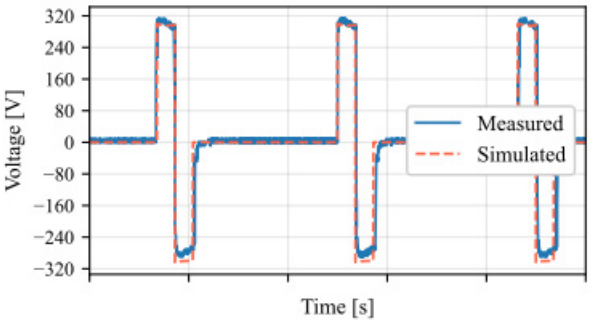


**Figure 16. Comparison between measured (blue) and simulated (dashed orange) values of induced voltage**

When the voltage undergoes rapid changes during the second half-cycle, i.e., when it assumes reverse polarity, discrete shifts in voltage level are expected. However, in the experimental measurements, a slight curvature is observed as it returns to zero (Fig. 17). This effect arises from the diodes' physical nonlinearity at low voltages and can be disregarded.

Additionally, another notable characteristic can be observed in Fig. 17: the induced voltage never drops to zero between two impulses. It takes a positive value bet–ween 0V and 8V that can't be determined precisely due to the oscilloscope's measurement discretization during the AC/DC conversion. This effect is also noticeable in the moment the switches close, when the voltage suddenly rises to 309V instead of the predicted 300V.

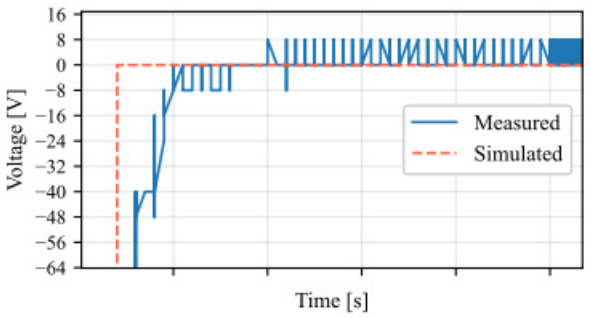


**Figure 17. Comparison between measured (blue) and simulated (dashed orange) values of induced voltage**

This effect could be considered just an error in the measurement process, but its source lies deeper in the electronics circuit of the EVA power supply. Given that

there is a small constant voltage in the circuit, when the switches are supposedly open, the current gradually increases. This effect can't be observed in oscilloscopic screen captures (Fig. 13 and Fig. 14). Still, it is clearly visible in the post-processed data of the readings of electrical current, that's given in Fig. 18. When the current's triangle impulse goes back to zero, the intensity of the electrical current rises and takes a value of 0.02A before the next triangle impulse starts. Even though the measured and simulated impulses' peaks coincide,the triangles of actual current impulses peak at 0.305A while the simulated ones peak at 0.343A.

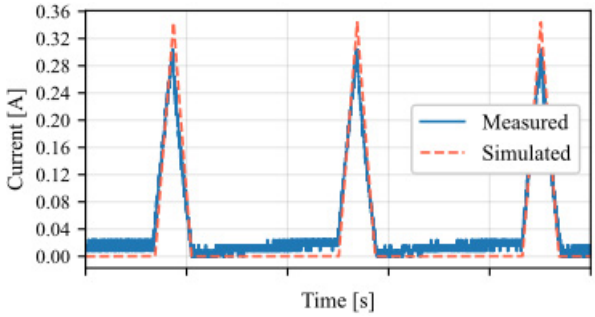


**Figure 18. Comparison between measured (blue) and simulated (dashedorange) values of electrical current**

Furthermore, a comparison between measured values and those obtained from numerical simulation is presented in Table 2. The absolute and relative errors of estimated values compared to values obtained with the laboratory experiment.

**Table 2. Comparison of the results of the numerical simulation and the values obtained during the laboratory experiment**

| Physicalvalue | Estimated value | Measured value | Absolute error | Relative error |
|---|---|---|---|---|
| Current's peak | 0.343A | 0.305A | 0.038A | 12.5% |
| Working stroke | 0.74mm | 0.67mm | 0.07mm | 10.5% |

## 8. CONCLUSION AND DISCUSSION

This research focuses on electromechanical energy conversion within an EVA during operation. Unlike previous studies [19-21], that decouple electrical from mechanical dynamics, the approach presented in this paper accounts for their nonlinear interaction. Furthermore, previous approaches often develop mathematical models for the specific case of EVA, e.g., treating it as a single-degree-of-freedom oscillator or neglecting gravity. In contrast, the presented mathematical model considers the general case, in which the size of the electromagnet's air gap is determined by the dynamics of the electromagnet armature's relative motion.

This study models the EVA with three state variables: the armature's relative velocity and displacement, and the electrical current flowing through the copper coil. Several previous studies adopt a similar approach but don't treat the current as a state variable; instead, they treat it as a control variable, i.e., an independently controllable quantity. This approach demonstrates the interdependencies between the electrical current and the dynamic properties of the aramture, thereby proving that the current can't be considered a control quantity. Unlike prior models, which often rely on various approximations, this approach considers variable inductance and the resistance of the copper coil.

The proposed mathematical model was validated with numerical simulation and a laboratory experiment on a laboratory prototype of a vibratory conveyor. During the experiment, the armature's displacement, electrical current, and induced voltage were measured and compared with results from numerical simulation, showing strong resemblance between the numerical simulation and the actual vibratory regime.

However, slight discrepancies can be observed between measured and estimated values, arising from the nonlinearity of EVA's power supply electronic circuit at low voltage levels, as the experimental setup was designed for high-voltage levels used in industrial environments. The comparison between the measured and estimated values shows relative errors of 12.5% for peak amplitudes of electrical current and 10.5% for the working stroke.Several factors contribute to the overall error metric: the experimental setup's poor performance at low voltages and the approximation of a three-dimensional electromagnetic field as a scalar equation. Magnetic flux fringing around the air gap was neglected, resulting in lower inductance. For lower estimated inductances, the current rises faster, hence the higher peak amplitudes. Consequently, as the electromagnetic force depends on the square of the current, higher excitation forces will result in larger displacements.

Furthermore, numerical simulation results provide insight into how various electrical quantities change during the observed vibratory regime (as shown in Fig. 12). This opens new possibilities for advanced sensor–less drive techniques that do not require an inductive sensor, in which only inductance is measured and current pulses are terminated accordingly. This concept represents a potential direction for future research, as well as the introduction of CAD/FEA tools for accurate three-dimensional modelling of electromagnetic fields, thereby incorporating magnetic flux fringing around the air gap.

## ACKNOWLEDGMENT

The results presented in this paper are part of the research supported by the Ministry of Science, Technological Development and Innovation, Republic of Serbia, contracts' number 451-03-136/2025-03/200034 and 451-03-137/2025-03/200105 from 04.02.2025.

## REFERENCES

[1] C. M. Franchi, Electrical Machine Drives: Fundamental Basics and Practice. CRC Press, 2019.

[2] V. S. Vasić, M. Lazarević, "Standard industrial guideline for mechatronic product design," FME Trans., vol. 36, no. 3, pp. 108–103, 2008.

[3] D. Rowell, D. N. Wormley, System Dynamics: An Introduction. Upper Saddle River, NJ: Prentice Hall, 1997.

[4] W. J. Palm, System Dynamics, 3rd ed. New York: McGraw-Hill Education, 2009.

[5] K. Ogata, System Dynamics, 4th ed. Upper Saddle River, NJ: Pearson Education, 2004.

[6] T. Todorov, R. Mitrev, B. Tudjarov, R. Nikolov, "Qualitative analysis of oscillating magnetomechanical system," IOP Conf. Ser. Mater. Sci. Eng., vol. 618, p. 012054, Oct. 2019.

[7] D. Markovic, N. Mladenovic, V. Simonovic, and I. Markovic, "Modeling the motion and mass quantity of fruit by rotating sizing machines," FME Transactions, vol. 42, no. 1, pp. 34–39, 2014

[8] U. Ilic, Ž. V. Despotović, "Modelling of the Magnetic Saturation Influence on the Electromagnetic force of the Vibratory Actuator / Modeliranje uticaja magnetnog zasićenja na elektromagnetnu silu vibracionog aktuatora," presented at the ENERGETIKA2024, Zlatibor, June 2024, p. 36.

[9] U. Ilić, Ž. V. Despotović, Modelling and Analysis of Magnetic Saturation Effects on the Electromagnetic Force in Vibratory Actuators, Energ. Ekon. Ekol., vol. 1, no. XXVII, pp. 11–15, 2025,

[10] A. Popović, B. Bojović, M. Suter, D. Niederer, "Design parameters effect to magnetic flux distribution of the reluctance actuator," FME Transactions, vol. 48, no. 3, pp. 504–510, 2020,

[11] V. Milošević-Mitić, A. Petrović, N. Anđelić, M. Jovanović, "The influence of temperature gradient on thin plates bending," FME Transactions, vol. 52, no. 1, pp. 128–135, 2024,

[12] M. Ristanović, D. Lazić, I. Inđin, "Experimental validation of improved performances of an electromechanical aerofin control system with a PWM controlled DC motor," FME Transactions, vol. 34, no. 1, pp. 20–15, 2006,

[13] M. M. Jovanović et al., "Experimental investigation of spillover effect in system of active vibration control," FME Transactions, vol. 42, no. 4, pp. 329–334, 2014,

[14] J. Liu, X. Zhang, X. Chen, "Modeling and active vibration control of a coupling system of structure and actuators," J. Vib. Control, vol. 22, pp. 382–395, Feb. 2016,

[15] A. R. Đorđević, Osnovi elektrotehnike 3. deo - elektromagnetizam. Akademska misao, 2016.

[16] A. R. Đorđević, Elektromagnetika. Akademska misao, 2012.

[17] V. Gourishankar, D. H. Kelly, Electromechanical Energy Conversion. New York: Intext Educational Publishers, 1973.

[18] I. F. Goncharevich, K. V. Frolov, E. I. Rivin, Theory of Vibratory Technology, 2nd ed. New York: Hemisphere Publishing Coorporation, 1990.

[19] A. I. Ribić, Ž. V. Despotović, "High-Performance Feedback Control of Electromagnetic Vibratory Feeder," IEEE Trans. Ind. Electron., vol. 57, no. 9, pp. 3087–3094, Sept. 2010,

[20] Ž. V. Despotović, D. Urukalo, M. R. Lečić, A. Ćosić, "Mathematical modeling of resonant linear vibratory conveyor with electromagnetic excitation: simulations and experimental results," Applied Mathematical Modelling., vol. 41, pp. 1–24, Jan. 2017,

[21] Z. Despotovic, M. Lecic, M. Jovic, A. Djuric, "Vibration control of resonant vibratory feeders with electromagnetic excitation," FME Transactions, vol. 42, no. 4, pp. 281–289, 2014,

[22] A. Cvetković, N. Trišović, L. Wei, "Simulation of the linear mechanical oscillator on GPU," FME Transactions, vol. 42, no. 4, pp. 317–322, 2014

[23] P. Krause, O. Wasynczuk, S. D. Sudhoff, S. Pekarek, Theory of Electromechanical Energy Conversion. IEEE, 2013.

[24] J. F. Gieras, Electrical Machines: Fundamentals of Electromechanical Energy Conversion. CRC Press, 2016.

[25] H. B. Callen, Thermodynamics and an Introduction to Thermostatistics, 2nd ed. Wiley, pp. 18-21, 1985.

[26] Y. A. Çengel, M. A. Boles, Thermodynamics: An Engineering Approach, 8th ed. McGraw-Hill Education, p. 70, 2015.

[27] C. W. T. McLyman, Transformer and Inductor Design Handbook, Third Edition. in Electrical and computer engineering Transformer and inductor design handbook. Taylor & Francis, 2004.

[28] U. Ilić, Ž. V. Despotović, M. Lazarević, E. Veg, "Modelling and Simulation of an Electromagnetic Vibratory Actuator Using CAD Software," in 2025 24th International Symposium INFOTEH-Jahorina, 2025, pp. 1–5.

[29] Z. V. Despotovic, Z. Stojiljkovic, "Power Converter Control Circuits for Two-Mass Vibratory Conveying System With Electromagnetic Drive: Simulations and Experimental Results," IEEE Transactions Industrial Electronics, vol. 54, no. 1, pp. 453–466, 2007,

[30] R.-F. Fung, Y.-T. Liu, C.-C. Wang, "Dynamic model of an electromagnetic actuator for vibration control of a cantilever beam with a tip mass," J. Sound Vib., vol. 288, no. 4, pp. 957–980, 2005,

[31] U. Lj. Ilić, M. P. Lazarević, E. A. Veg, Ž. V. Despotović, "Motion analysis of a vibratory conveyor's trough during its operation," in Proceedings, Serbian Society of Mechanics, Belgrade, 2025, pp. 196–205.

[32] Z. Golubović, M. Simonović, Z. Mitrović, Mehanika: Statika. Beograd: Mašinski fakultet Univerziteta u Beogradu, 2019.

[33] U. Ilić, M. Lazarević, "Applying Rodrigues' Formula for Kinematic Modeling of Vibratory Conveyors," presented at the 2nd International Conference on Mathematical Modelling in Mechanics and Engineering, Mathematical Institute SANU, Sept. 2024, pp. 59–60.

[34] F. Kipriyanov, P. Savinykh, A. Aleshkin, A. Isupov, "Experimental and mathematical modelling of grain material velocity," E3S Web Conf, vol. 381, 2023,

[35] A. Götzendorfer, J. Kreft, C. A. Kruelle, I. Rehberg, "Sublimation of a Vibrated Granular

Monolayer: Coexistence of Gas and Solid," Phys Rev Lett, vol. 95, no. 13, p. 135704, Sept. 2005,

[36] B. Balachandran, E. B. Magrab, Vibrations, 2nd ed. Australia: Cengage Learning, 2009.

[37] N. Jafari, M. Azhari, "Free vibration analysis of viscoelastic plates with simultaneous calculation of natural frequency and viscous damping," Math. Comput. Simul., vol. 185, pp. 646–659, 2021,

[38] X. Zou, B. Zhang, G. Yin, "Analysis of stiffness and damping performance of the composite leaf spring," Sci. Rep., vol. 12, no. 1, p. 6842, Apr. 2022,

## ЕЛЕКТРОМЕХАНИЧКО ПРЕТВАРАЊЕ ЕНЕРГИЈЕ УНУТАР ЕЛЕКТРОМАГНЕТНОГ ВИБРАЦИОНОГ АКТУАТОРА: МОДЕЛИРАЊЕ, СИМУЛАЦИЈА И ВАЛИДАЦИЈА

**У.Љ. Илић, Ж.В. Деспотовић, М.П. Лазаревић, Е.А. Вег**

У оквиру рада описан је развој и валидација нелинеарног математичког модела електромаг–нетног вибрационог актуатора, који је заступљен у вибрационим транспортерима. Мотивација за ово истраживање проистиче из потребе за детаљнијим разумевањем феномена електромеханичког претва–рања енергије, који се дешава током експлоатације једног електормагнетног вибрационог актуатора. За разлику од досадашних математичких модела, који често бивају моделирани помоћу линеарних апрок–симација или засебним разматрањем механике и електродинамике актуатора, предложени модел има за циљ интеграцију нелинеарних електромагнених ефеката са динамиком релативног кретања котве електромагнета, тако успостављајући зависност између електричних величина у струјном колу и динамичких карактеристика покретног елемента електромагнета. Новодобијени математички модел је симулиран помоћу нумеричких симулација, при чему су параметри модела узети по узору на функ–ционални лабораторијски прототим. На крају је описана и експериментална валидација, која пока–зује значајно слагање са симулационим резултатима.